

Original scientific paper

EFFECTS OF ROTATION ON UNSTEADY FLUID FLOW AND FORCED CONVECTION IN THE ROTATING CURVED SQUARE DUCT WITH A SMALL CURVATURE

Mohammad Sanjeed Hasan¹, Ratan Kumar Chanda²,
Rabindra Nath Mondal², Giulio Lorenzini³

¹Department of Mathematics, Bangabandhu Sheikh Mujibur Rahman Science and Technology University, Gopalganj, Bangladesh

²Department of Mathematics, Jagannath University, Dhaka, Bangladesh

³Department of Engineering and Architecture, University of Parma, Parma, Italy

Abstract. *In recent years, the analysis of flow disposition in a curved duct (CD) has greatly attracted researchers because it is broadly used in engineering devices. In the present paper, unsteady flow characteristics of energy transfer (HT) in a rotating curved square duct (CSD) have been presented with the aid of spectral method. The key purpose of this study is to explore rotational effects and heat transfer (HT) of the duct. For this purpose, time-evolution calculation is performed over the Taylor number ($-1500 \leq Tr \leq 1500$) and other parameters are fixed; e.g., Dean number ($Dn = 1000$), Curvature ($\delta = 0.015$) and Prandtl number ($Pr = 7.0$, for water). Firstly, time-dependent behavior is accomplished for both clockwise and anticlockwise rotations. It is found that the flow instabilities are certainly governed by the change of Tr that has been justified by sketching phase spaces (PS). To observe the flow features, velocities including axial flow (AF), secondary flow (SF) and temperature profiles are disclosed for both rotations; and it is elucidated that 2- to 6-vortex solutions are generated for physically realizable solutions. Axial flow (AF) shows that two maximum-velocity regimes are produced which induces secondary flow (SF), and, consequently, a strong bonding between the AF and SF has been built up. It is observed that as the rotation is increased, the fluid is mixed considerably which boosts HT in the fluid. Finally, an assessment between the numerical and experimental data has been given, and a good agreement is observed.*

Key Words: *Rotating Curved Duct, Taylor Number, Heat-flux, Phase Space, Chaos*

Received January 29, 2021 / Accepted May 10, 2021

Corresponding author: Mohammad Sanjeed Hasan

Department of Mathematics, Bangabandhu Sheikh Mujibur Rahman Science and Technology University, Gopalganj-8100, Bangladesh

E-mail: sanjeedlhasan@gmail.com

1. INTRODUCTION

The investigation of developed fluid flows behavior and HT through a rotating curved duct (RCD) and like constrained domains is of essential interest of a great many researchers because of a multitude of its applications in the engineering fields, e.g., in transporting fluids, rotating-machinery, metallic industry, nuclear engineering, heat exchangers, gas turbines, electric generators, rocket engines and blade-to-blade passage for cooling systems. Numerous investigations into different types of ducts have been studied by many authors. Among them, Mondal et al. [1, 2] (square duct) and Yanase et al. [3] (rectangular duct), Rumsey et al. [4] (U-duct), Chandratilleke et al. [5] (rectangular and elliptical duct), Ahmadloo et al. [6] (helical pipe) can be mentioned as outstanding analyses.

One of the prominent features in analyzing curved ducts refers to examination of steady and unsteady flow characteristics. Symmetric and asymmetric steady solution branches for a tightly coiled duct were gained by Liu and Wang [7]. They disclosed the structural displacements of bifurcation for changing the grid points and analyzed stability. Besides, they calculated the dynamical responses for several pseudo-Dean numbers. Yanase et al. [8] used two-dimensional geometry to study transitional behavior for the CD flow with large varying aspect ratios. Later, Yanase et al. [9] carried out a three-dimensional coordinate system to explore the same analysis for non-rotating CSD; then they differentiated their results from the previous ones. The US regarding the resistance coefficient and the fluid velocity for several Reynolds numbers and gap spacing parameters across multiple staggered rows of cylinders have been represented by Nazeer et al. [10]. They validated their periodic oscillation by the power spectrum analysis. Zhou et al. [11] used the PIV method to compare the unsteady flow characteristics in a half and fully dimpled circular cylinder for large Reynolds numbers. Zhang et al. [12] conducted unsteady behavior for four square-shaped cylinders where the cylinders were kept at an equal distance from each other. Hashemi et al. [13] measured the fluctuation of the velocity components regarding time through the curved pipe. Unsteady behaviors in a square enclosure with mixed convection have been steered out by Zhang et al. [14]. Wang and Yang [15] numerically and experimentally reported dynamical responses of the flow through the CD for various Dn . Transient behaviors with thermal analysis in porous cavities for large aspect ratios have been calculated by Arpino et al. [16]. Mondal et al. [17, 18] computed the change of unsteady flow behavior, justifying by PS of US results, in the cooling and heating sidewalls for several Dn , Gr , Ar and Tr numbers, respectively. Hasan et al. [19, 20] obtained three different types of flow oscillations such as steady-state, periodic, and chaotic flow for both rotating and non-rotating CD with small and moderate curvatures, respectively. Islam et al. [21] adopted function expansion and collocation method to seek out the USs for rotating curved rectangular duct (CRD) flow. Kurtulmus et al. [22] observed the Nusselt number effect in flow transition for converging and diverging channel. Zheng et al. [23] used $k - \omega$ turbulence model in a serpentine tube to obtain the temperature oscillation and the effects of centrifugal and buoyancy force in the flow transition. Among the cited papers, most of the authors showed only flow transition; some of them investigated power spectrum density to justify the flow oscillation. But they did not illustrate the phase space which is an important phenomenon for regular and irregular flow transition. The present study, therefore, represents unsteady flow characteristics, and the flow transition is meticulously justified by sketching PS of the time change of flux that gives a clear view for the regular and irregular oscillation.

Flow visualization is another significant material for the duct because it recounts the effects of fluid and heat transfer mixing. It is known that Dean [24] was the first who

derived the governing equations of curved ducts. He related that the double-vortex secondary velocity converted into the quadruple-vortex one at the limit points of the steady solution and these two-vortices are named after him: the *Dean vortices*. He demonstrated that there are three types of potency such as centrifugal force, Coriolis force and body force working in the fluid flow. Here, it is noted that the centrifugal and Coriolis forces are influenced by the duct curvature and rotation, respectively. Ozaki and Maekawa [25] showed curvature effects in the curved duct flow. Numerical and experimental investigations with heat transfer through curved rectangular and elliptical ducts were illustrated by Chandratilleke et al. [26]. Ferdows et al. [27] explained the effects of the Dean number in the helical duct for different rotational numbers. Bayat et al. [28] developed numerical and experimental flow model to demonstrate the upshot of curvature and kinematic viscosity for curved and spiral micro-channel. Li et al. [29] pursued the numerical study of two-dimensional flow behavior for changing the curvature and Ar of the duct. Li et al. [29] pursued the numerical study of two-dimensional flow behavior for changing the bend and size of the channel. They further represented the three-dimensional stream-flow velocity where the flow fields were measured by using the particle image velocimetry technique. Watanabe and Yanase [30] attempted to develop a 3-D model to visualize the flow structures. Nowruzi et al. [31] used the energy gradient method to report flow structure through a CRD with 120° inlet. Considering the perturbation method as the main tool, Norouzi and Biglari [32] accomplished the formation of secondary flow structures. They further sketched the vector plot of the secondary flow. Razavi et al. [33] performed flow structure, heat and entropy transmission through a rotating curved channel where they applied the second law of thermodynamics. The influence of centrifugal and hydrodynamic instability in the flow transition and heat conduction was attained by Hasan et al. [34, 35]. Sasmito et al. [36] evaluated the enhancement of heat transfer for the nano-fluid particle in coiled ducts. Al-Juhaishi et al. [37] elucidated the friction losses and heat generation in a curved duct. They demonstrated that heat transfer is dramatically induced by the baffles of the channel. Zhang et al. [38] suggested a 3D scheme to show the impact of centrifugal force on the heat flow across the curve tube. Zhang et al. [39] illustrated the chaotic flow and energy distribution under a critical buoyancy and rotation numbers. Schindler et al. [40] calculated the total amount of heat transfer and the fluid mixing when the turbulent flows occurred in a heated CSD. However, it is clear that the AF and SF velocity and the isotherms have a close interaction, which has not been explored in literature till today. The ongoing paper, therefore, represents a strong connection between the flow velocity and the isotherms together with the transitional flow characteristics and energy transfer in the duct.

2. PHYSICAL MODEL AND MATHEMATICAL FORMULATION

Fig. 1 presents the present study considering a two-dimensional (2D) scheme of a curved duct with constant curvature as well as a laminar flow passing through the duct. The temperature difference is kept between two horizontal duct walls in which the lower wall is heated while the upper wall is cooled. The co-ordinate system with relevant notations is shown in Fig. 1.

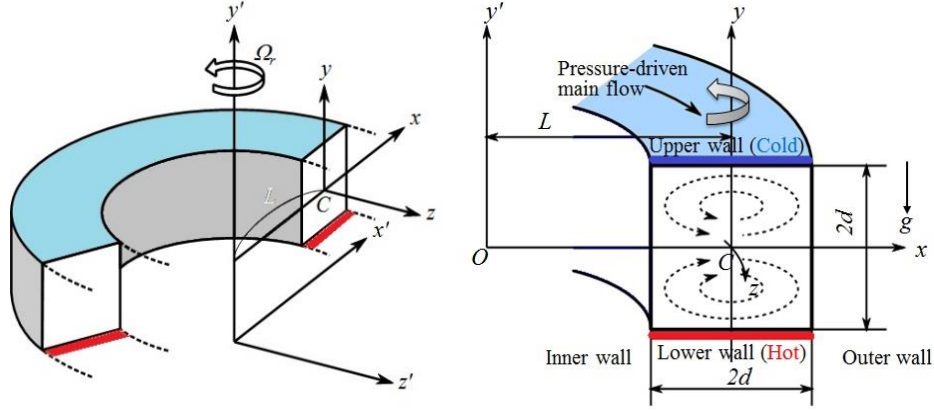


Fig. 1 (a) Physical domain (b) Cross-section of the system

The set of controlling equations is given as:

Continuity equation:

$$\frac{\partial v_r}{\partial r} + \frac{1}{r} \frac{\partial v_\theta}{\partial \theta} + \frac{\partial v_y}{\partial y} + \frac{v_r}{r} = 0 \quad (1)$$

Momentum equations:

$$\frac{\partial v_r}{\partial t} + (v \cdot \nabla) v_r - \frac{v_\theta^2}{r} = -\frac{1}{\rho} \frac{\partial P}{\partial r} + \nu \left(\tilde{\Delta} v_r - \frac{v_r}{r^2} - \frac{2}{r^2} \frac{\partial v_\theta}{\partial \theta} \right) \quad (2)$$

$$\frac{\partial v_\theta}{\partial t} + (v \cdot \nabla) v_\theta + \frac{v_r v_\theta}{r} = -\frac{1}{\rho r} \frac{\partial P}{\partial \theta} + \nu \left(\tilde{\Delta} v_\theta - \frac{v_\theta}{r^2} + \frac{2}{r^2} \frac{\partial v_r}{\partial \theta} \right) \quad (3)$$

$$\frac{\partial v_y}{\partial t} + (v \cdot \nabla) v_y = -\frac{1}{\rho} \frac{\partial P}{\partial y} + \nu \tilde{\Delta} v_y + \beta g T \quad (4)$$

Energy equation:

$$\frac{\partial T}{\partial t} + (v \cdot \nabla) T = \kappa \tilde{\Delta} T \quad (5)$$

Here:
$$v \cdot \nabla = v_r \frac{\partial}{\partial r} + \frac{v_\theta}{r} \frac{\partial}{\partial \theta} + v_y \frac{\partial}{\partial y}, \quad \tilde{\Delta} = \frac{\partial^2}{\partial r^2} + \frac{1}{r} \frac{\partial}{\partial r} + \frac{1}{r^2} \frac{\partial^2}{\partial \theta^2} + \frac{\partial^2}{\partial y^2}$$

where v_x , v_y , and v_θ are velocity components along axes r , y , and θ , respectively.

To make dimensional Eqs. (1-5) into dimensionless by defining the following variables,

$$r = L + dx', \quad y = h \times y', \quad L \times \theta = -dz', \quad T = T' \times \Delta T, \quad v_r = v_x = U_0 \times u', \quad v_y = v_y = U_0 \times v',$$

$$v_\theta = -v_z = U_0 \times w', \quad \rho = \rho_0 U_0^2 P', \quad G = -\frac{\partial P'}{\partial z'}, \quad \epsilon = \sqrt{\frac{2d}{L}} = \sqrt{2\delta}, \quad \delta = \frac{d}{L}$$

The proportion of width to the duct curvature radius is curvature (δ). Since the present study is 2-D flow which passes uniformly in the axial direction so $\partial p'/\partial z' = 0$. The derived equation is as follows:

Continuity equation:

$$\frac{\partial u'}{\partial x'} + \frac{\partial v'}{\partial y'} + \frac{\delta u'}{\beta'} + \frac{1}{\beta'} \frac{\partial w'}{\partial z'} = 0 \quad (6)$$

Momentum equations:

$$\frac{\partial u'}{\partial t'} + (v' \cdot \nabla) u' - \frac{1}{2} \epsilon^2 \frac{w'^2}{\beta'} = -\frac{\partial P'}{\partial x'} + \frac{\epsilon}{Dn} \left(\tilde{\Delta}'_2 u' - \frac{\delta^2 u'}{\beta'^2} \right) \quad (7)$$

$$\frac{\partial v'}{\partial t'} + (v' \cdot \nabla) v' = -\frac{\partial P'}{\partial y'} + \frac{\epsilon}{Dn} \tilde{\Delta}'_2 v' + \frac{\beta g \Delta T l}{U_0^2} T' \quad (8)$$

$$\frac{\partial w'}{\partial t'} + (v' \cdot \nabla) w' + \frac{1}{2} \epsilon^2 \frac{u' w'}{\beta'} = -\frac{G}{\beta'} + \frac{\epsilon}{Dn} \left(\tilde{\Delta}'_2 w' - \frac{\delta^2 u'}{\beta'^2} \right) \quad (9)$$

Energy equation:

$$\frac{\partial T'}{\partial t'} + (v' \cdot \nabla) T' = \frac{\kappa}{dU_0} \tilde{\Delta}'_2 T' \quad (10)$$

where,

$$\beta' = 1 + \delta x', \quad (v' \cdot \nabla) = u' \frac{\partial}{\partial x'} + v' \frac{\partial}{\partial y'} \quad \text{and} \quad \tilde{\Delta}'_2 = \frac{\partial^2}{\partial x'^2} + \frac{\partial}{\partial y'^2} + \frac{\delta}{\beta'} \frac{\partial}{\partial x'}$$

The vorticity vector can be written as

$$\Omega = \frac{\partial v'}{\partial x'} - \frac{\partial u'}{\partial y'} = -\frac{1}{\beta'} \left(\frac{\partial^2}{\partial x'^2} + \frac{\partial^2}{\partial y'^2} - \frac{\delta}{\beta'} \frac{\partial}{\partial x'} \right) \quad (11)$$

and stream function as

$$u' = \frac{1}{\beta'} \frac{\partial \psi'}{\partial y'} \quad \text{and} \quad v' = -\frac{1}{\beta'} \frac{\partial \psi'}{\partial x'} \quad (12)$$

Now subtracting $\frac{\partial}{\partial y'}$ (9) from $\frac{\partial}{\partial x'}$ (8), we obtain the equation:

$$\begin{aligned} \frac{\partial \Omega}{\partial t'} + \left(u' \frac{\partial}{\partial x'} + v' \frac{\partial}{\partial y'} \right) \Omega - \frac{\delta u'}{\beta'} \Omega + \frac{\epsilon^2 w'}{\beta'} \frac{\partial w'}{\partial y'} \\ = \frac{\epsilon}{Dn} \left(\tilde{\Delta}'_2 - \frac{\delta^2}{\beta'} \right) \Omega + \frac{\beta g \Delta T l}{U_0^2} \frac{\partial T'}{\partial x'} \end{aligned} \quad (13)$$

Then, moderated equations for w , ψ and T as follows (removing (' sign) are:

$$\beta \frac{\partial w}{\partial t} + \frac{\partial(w, \psi)}{\partial(x, y)} - Dn + \frac{\delta^2 w}{\beta} = \beta \Delta_2 w - \frac{\delta w}{\beta} \frac{\partial \psi}{\partial y} + \delta \frac{\partial w}{\partial x} - \delta Tr \frac{\partial \psi}{\partial y}, \quad (14)$$

$$\begin{aligned} \left(\Delta_2 - \frac{\delta}{\beta} \frac{\partial}{\partial x} \right) \frac{\partial \psi}{\partial T} &= -\frac{1}{\beta} \frac{\partial(\Delta_2 \psi, \psi)}{\partial(x, y)} + \frac{\delta}{\beta^2} \left[3\delta \frac{\partial^2 \psi}{\partial x^2} - \frac{3\delta^2}{\beta} \frac{\partial \psi}{\partial x} \right] \\ -\frac{2\delta}{\beta} \frac{\partial}{\partial x} \Delta_2 \psi + \frac{\delta}{\beta^2} \left[\frac{\partial \psi}{\partial y} \left(2\Delta_2 \psi - \frac{3\delta}{\beta} \frac{\partial \psi}{\partial x} + \frac{\partial^2 \psi}{\partial x^2} \right) - \frac{\partial \psi}{\partial x} \frac{\partial^2 \psi}{\partial x \partial y} \right] &+ w \frac{\partial w}{\partial y} \\ + \Delta_2^2 \psi - Gr \times \beta \frac{\partial T}{\partial x} + \frac{1}{2} Tr \frac{\partial w}{\partial y}, & \end{aligned} \quad (15)$$

$$\frac{\partial T}{\partial t} + \frac{1}{\beta} \frac{\partial(T, \psi)}{\partial(x, y)} = \frac{1}{Pr} \left(\Delta_2 T + \frac{\delta}{\beta} \frac{\partial T}{\partial x} \right), \quad (16)$$

where,

$$\Delta_2 = \frac{\partial^2}{\partial x^2} + \frac{\partial^2}{\partial y^2}, \quad \beta = 1 + \delta x \quad \text{and} \quad \frac{\partial(P, Q)}{\partial(x, y)} = \frac{\partial P}{\partial x} \frac{\partial Q}{\partial y} - \frac{\partial P}{\partial y} \frac{\partial Q}{\partial x}$$

The non-dimensional parameters that characterize the flow appear in Eqs. (14-16): Dean number, $Dn \left(= \frac{Gd^3}{\mu \nu} \sqrt{\frac{2d}{L}} \right)$, Taylor number, $Tr \left(= \frac{2\sqrt{2}\delta\Omega_T d^3}{\nu\delta} \right)$, Grashof number, $Gr \left(= \frac{\beta g \Delta T d^3}{\nu^2} \right)$ and Prandtl number, $Pr \left(= \frac{\nu}{\kappa} \right)$.

The boundary conditions for w and ψ are

$$\left. \begin{aligned} w = \psi = \frac{\partial \psi}{\partial x} = 0, x = \pm 1, y = y \\ w = \psi = \frac{\partial \psi}{\partial y} = 0, x = x, y = \pm 1 \end{aligned} \right\} \quad (17)$$

and for temperature T are considered as

$$\left. \begin{aligned} T = 1, x = x, y = 1 \\ T = -1, x = x, y = -1 \\ T = y, x = \pm 1, y = y \end{aligned} \right\} \quad (18)$$

The considered fluid is water ($Pr = 7.0$), and we run computational simulations for $Dn = 1000$, $Gr = 100$, $\delta = 0.015$, and $Tr \in [-1500, 1500]$.

3. NUMERICAL ANALYSIS

3.1. Numerical Procedure

Since the method is numerically based, we have used the Spectral method as a numerical technique to solve the Eqs. (14-16). This is the best method for solving the Navier-Stokes as well as energy equations (Gottlieb and Orszag [41] and Mondal [42]). By this method the

variables are expanded into a series of functions consisting of Chebyshev polynomials. Expansion functions $\mu_n(\eta)$ and $\phi_n(\eta)$ are stated as

$$\left. \begin{aligned} \mu_n(\eta) &= (1-\eta^2) F_n(\eta), \\ \phi_n(\eta) &= (1-\eta^2)^2 F_n(\eta) \end{aligned} \right\} \quad (19)$$

where, $F_n(\eta) = \cos(ncos^{-1}(\eta))$ is the n^{th} order Chebyshev polynomials. Furthermore, $w(\eta, \gamma, t)$, $\psi(\eta, \gamma, t)$ and $T(\eta, \gamma, t)$ are expanded in terms of $\mu_n(\eta)$ and $\phi_n(\eta)$ as:

$$\left. \begin{aligned} w(\eta, \gamma, t) &= \sum_{m=0}^M \sum_{n=0}^N w_{mn}(t) \mu_m(\eta) \mu_n(\gamma) \\ \psi(\eta, \gamma, t) &= \sum_{m=0}^M \sum_{n=0}^N \psi_{mn}(t) \phi_m(\eta) \phi_n(\gamma) \\ T(\eta, \gamma, t) &= \sum_{m=0}^M \sum_{n=0}^N T_{mn}(t) \mu_m(\eta) \mu_n(\gamma) - \gamma \end{aligned} \right\} \quad (20)$$

where M and N represent the truncation numbers along the x -and y -directions, respectively. In order to obtain the nonlinear algebraic equations for expansion coefficients w_{mn} , ψ_{mn} and T_{mn} , the expansion coefficients have been substituted into the Eqs. (14-16) and the collocation method is applied. Collocation points (x_i, y_j) are taken to be

$$\left. \begin{aligned} x_i &= \cos \left[\pi \left(1 - \frac{i}{M+2} \right) \right], \quad i=1, \dots, M+1 \\ y_j &= \cos \left[\pi \left(1 - \frac{j}{N+2} \right) \right], \quad j=1, \dots, N+1 \end{aligned} \right\} \quad (21)$$

To obtain the time-dependent evolution of w_{mn} , ψ_{mn} , and T_{mn} , we substitute the required series expansion (20) into basic Eqs. (14-16).

3.2. Flux through the Duct

The flux representing total flow in a curved duct is calculated by the following formula

$$Q' = \int_{-d}^d \int_{-d}^d w' dx' dy' = VdQ \quad (22)$$

where, Q : dimensional heat-flux; \bar{w}' : mean axial velocity which is defined by

$$\bar{w}' = \frac{Qv}{4d} \quad (23)$$

Converting the dimensional Eq.(22) into a non-dimensional form, flux Q is formulated as

$$Q = \int_{-1}^1 \int_{-1}^1 w dx dy \quad (24)$$

3.3. Grid Efficiency

Table 1 The values of Q and $w(0, 0)$ for various M and N at $Dn = 1000$, $Gr = 100$, $Tr = 500$ (positive rotation) and $Tr = -500$ (negative rotation) and $\delta = 0.015$

| | M | N | Q | $w(0,0)$ |
|----------------------|-----------|-----------|-----------------------|-----------------------|
| Positive Rotation | 16 | 16 | 291.1740208493 | 382.6415407505 |
| | 18 | 18 | 291.4440637777 | 378.9279648439 |
| | 20 | 20 | 291.5043954187 | 378.2773776991 |
| | 22 | 22 | 291.5491957619 | 379.0478252693 |
| | 24 | 24 | 291.5511087350 | 379.0911636619 |
| Negative Rotation | 16 | 16 | 322.2820420248 | 381.0710697212 |
| | 18 | 18 | 322.2817278220 | 381.0904822522 |
| | 20 | 20 | 322.2795158289 | 381.3121404054 |
| | 22 | 22 | 322.2790330741 | 381.4151170197 |
| | 24 | 24 | 322.2787357133 | 381.5126278631 |

Here, grid efficiency is carried out for truncation numbers M and N . As the research deals with square duct flow, so M and N are considered as equal. In this study, the values of axial flow and heat flux for both co-rotation and counter-rotation are taken for different truncation numbers where the parameters of governing equations are fixed. Table 1 shows grid accuracy; it can be seen that the values do not show any substantial change for increasing or decreasing the truncation numbers. To get sufficient accuracy, $M = (N) = 20$ has been taken for numerical simulation.

4. RESULTS

In the following discussion, transitional behavior of the fluid flow is performed for fixed Grashof number, $Gr (= 100)$; curvature, $\delta (= 0.015)$ and Dean number, $Dn (= 1000)$ and parameter Tr (Taylor number); geometric significance is duct rotation, varied from 1500 to 1500. The programming algorithm of the governing equations is developed by allocating three methods including the Crank-Nicolson, Adam-Bashforth, and function collocation method simultaneously. Moreover, the characteristics of the axial velocity, secondary flow and energy distribution from contour plots for co-rotation and counter-rotation have also been explored in this study.

4.1. Time-dependent Flow Behaviors

4.1.1. Case I: Co-rotation ($0 \leq Tr \leq 1500$)

Initially, we consider Taylor number $Tr = 10$. The time-dependent of the unsteady solution (US) is analyzed and found that the unsteady flow gives a multi-periodic solution in $t - Q$ plane as plotted in Fig. 2(a). The recognition of multi-periodicity is examined by the phase space (PS) analysis as depicted in Fig. 2(b). Here, the PS is calculated from the unsteady solution and sketched in the $\lambda - \gamma$ plane, where γ is prescribed by $\gamma = \int \int \psi dx dy$. The phase space in Fig. 2(b) narrates the ability of the tremble as a function of frequency at which the frequencies have potent and at which the frequencies are feeble. Axial velocity, stream function and isotherms are shown in Fig. 3. The observation from the AF is that the particle

has pressed opposite to the duct's outer circumference. From the stream function, 2- to 4-vortex solution is found for $Tr = 10$. It is found that the axial velocity and the stream function have a close bond. At $t = 26.00$ and $t = 26.30$, two high-velocity portions are produced at the outer circumference of the bend; as a result, two new vortices are generated. Here, the newly-produced two-vortices are known as *Dean vortices* and the previous two-vortices are called *Ekman vortices*. It is further illustrated that the two new vortices at $t = 26.00$ are smaller than those at $t = 26.30$. This has happened because of the influence of the axial flows. More explicitly, at $t = 26.00$, only a pair of high-velocity regions are created at the outer circumference where no dumbbells are formed. On the other hand, at $t = 26.30$, a pair of high velocity regions are generated with a pair of dumbbells at the left-top and left-bottom of the enclosure. As a result, newly-created two vortices at $t = 26.30$ are larger than the two vortices formed at $t = 26.00$. It is also remarked that, due to dumbbells at $t = 26.30$, the flow velocity is stronger than that at $t = 26.00$ due to the centrifugal force of the duct. Temperature profiles show that heat is transferred exceedingly at $t = 26.00$ and $t = 26.30$ within the time ($25.90 \leq t \leq 26.40$). It is easily demonstrated that when the flow velocity is strong, more heat is transferred which proves that the fluid is mixed excessively when the velocity of the flows is strong.

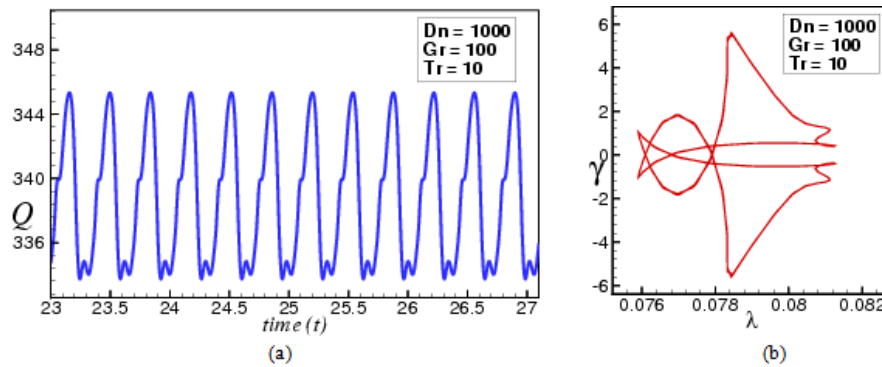


Fig. 2 Transient solution for $Tr = 10$ (a) Q as a function of time, (b) PS of (a)

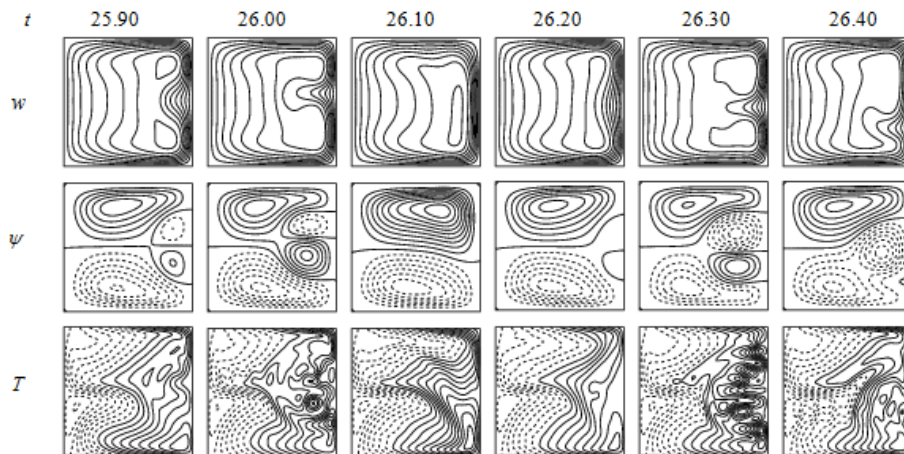


Fig. 3 Velocity contour (top & middle) and isotherm (bottom) for $Tr = 10$

If the rotational speed is extended, the multi-periodic flow converts into a steady-state solution. Fig. 4(a) shows steady-state solutions for $Tr = 200$ and $Tr = 400$. In the region $200 \leq Tr \leq 400$, as we increase the value of the Taylor number, the heat-flux value decreases and the steady-state solutions are organized accordingly. Axial velocity, stream function and isotherm are visualized in Fig. 4(b) and found only symmetric 2-vortex secondary flow patterns.

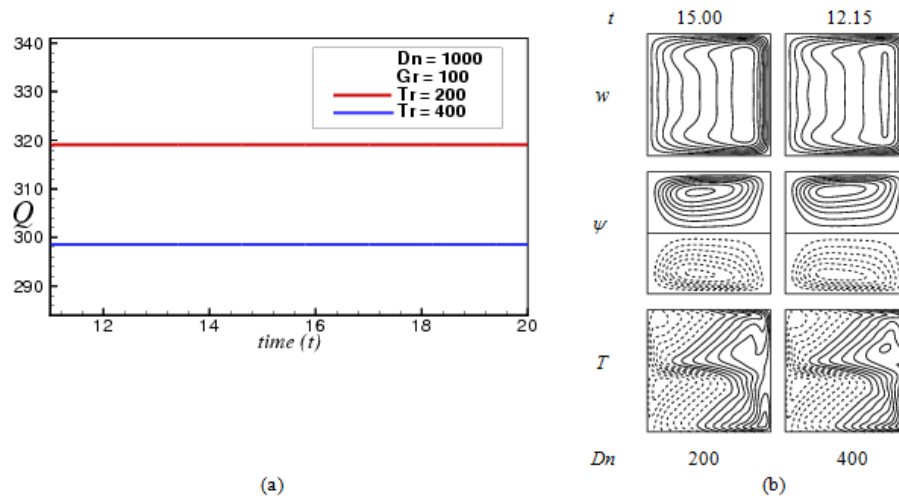


Fig. 4 Transient solution for $Tr = 200$ and $Tr=400$ (a) Q as a function of time, (b) Velocity contour (top & middle) and isotherm (bottom)

Regular oscillation starts for $Tr > 750$. Here, we investigate time-development of the US for $Tr = 900$ and the outcomes are plotted in Fig. 5(a) which indicates the periodic oscillation. To ensure it more, PS is also computed as displayed in Fig. 5(b). The path line of the PS, displaying multiple orbits, can show that the flow is in the initial stage of a multi-periodic oscillation instead of the periodic oscillation created at $Tr = 900$. This has occurred because the flow characteristics are significantly affected by the Coriolis force. The AF, asymmetric 2-vortex stream function and isotherm are shown in Fig. 6.

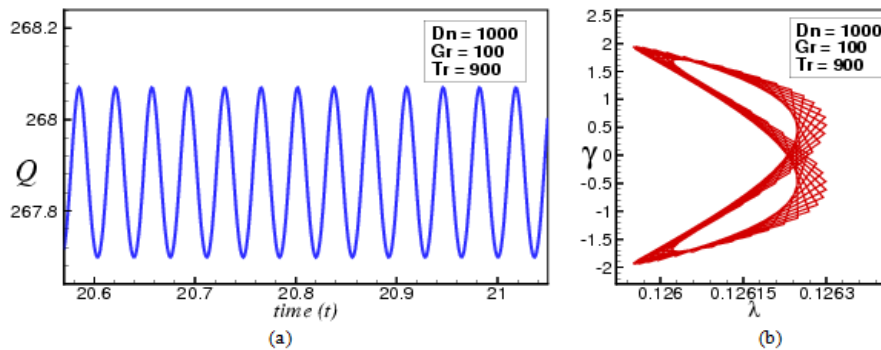


Fig. 5 Transient solution for $Tr = 900$ (a) Q as a function of time, (b) PS of (a)

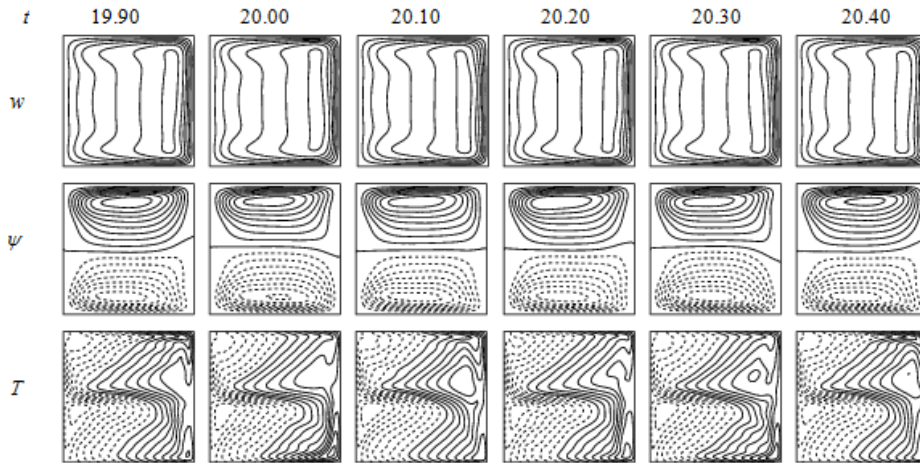


Fig. 6 Velocity contour (top & middle) and isotherm (bottom) for $Tr = 900$

Due to disorientation in periodic and multi-periodic flow, we investigate time-dependent solution from $Tr = 950$ to $Tr = 1300$. It is elucidated that the oscillation for the required Tr is certainly multi-periodic. Fig. 7(a) represents the multi-periodic flow for $Tr = 1300$. The PS drawn in Fig. 7(b) shows that multiple orbits are produced and the path lines overlap with each other. It is further expressed that the area of stream function is growing for increasing Tr . So, it can be said that the multi-periodic oscillation is nearly at the terminal stage. Flow patterns with isotherms are drawn (see Fig. 8). It is noticed that 2-vortex asymmetric secondary flow is created at $Tr = 1300$ where the axial flow and the temperature profiles bear their usual significances.

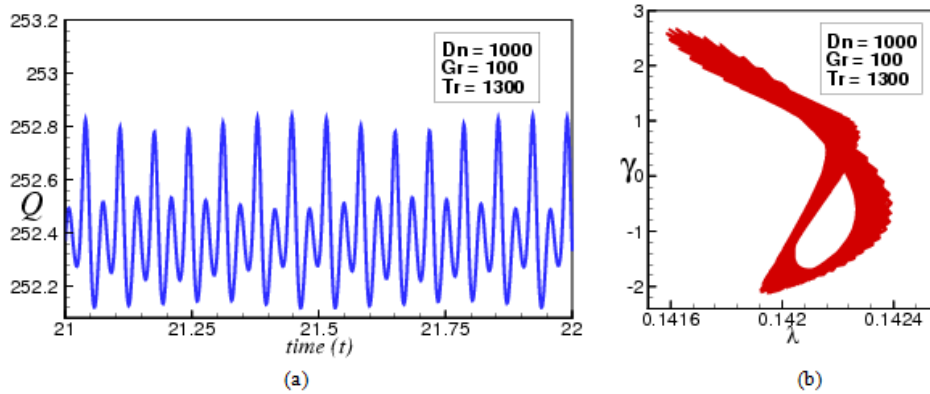


Fig. 7 Transient solution for $Tr = 1300$ (a) Q as a function of time, (b) PS of (a)

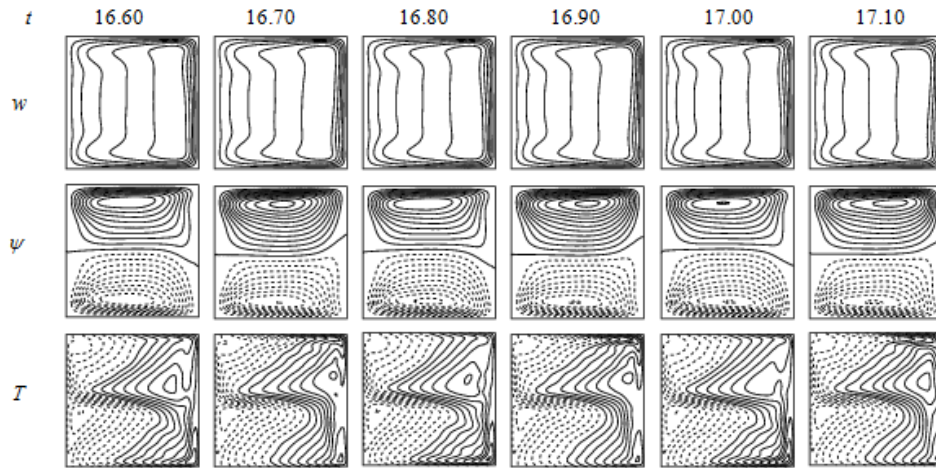


Fig. 8 Velocity contour (top & middle) and isotherm (bottom) for $Tr = 1300$

If Tr is raised more, the multi-periodic flow transforms into an irregular oscillation i.e., the flow is chaotic. The chaotic oscillation starts at $Tr = 1350$ approximately and continues till $Tr = 1500$. The characteristics of the unsteady flow for $Tr = 1450$ are shown in Fig. 9(a). It is observed that the flow oscillates more at the irregular (chaotic) flow than the regular (periodic/ multi-periodic) oscillation and the density of the oscillation enhances as Tr increases. PS of the chaotic oscillations is also enumerated (see Fig. 9(b)), which justifies the flow configuration as it was anticipated. From the phase space, the path lines pass over each other in the $\lambda - \gamma$ plane; as a result, a critical flow characteristic has been found. It can be said that due to increase of Tr , the flow oscillation is enhanced gradually. As a consequence, the vibration of fluid particle increases, for this reason; the fluid particles are amalgated which prolongs the overall heat transfer in flow. Axial velocity, stream function and isotherms are depicted in Fig. 10 for $Tr = 1450$.

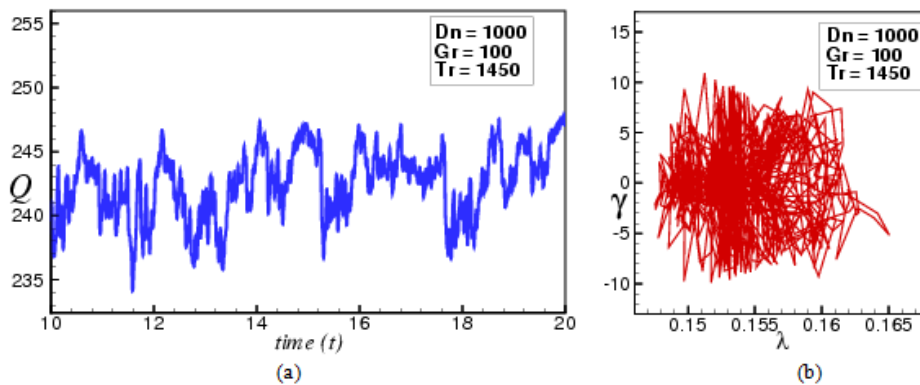


Fig. 9 Transient solution for $Tr = 1450$ (a) Q as a function of time, (b) PS of (a)

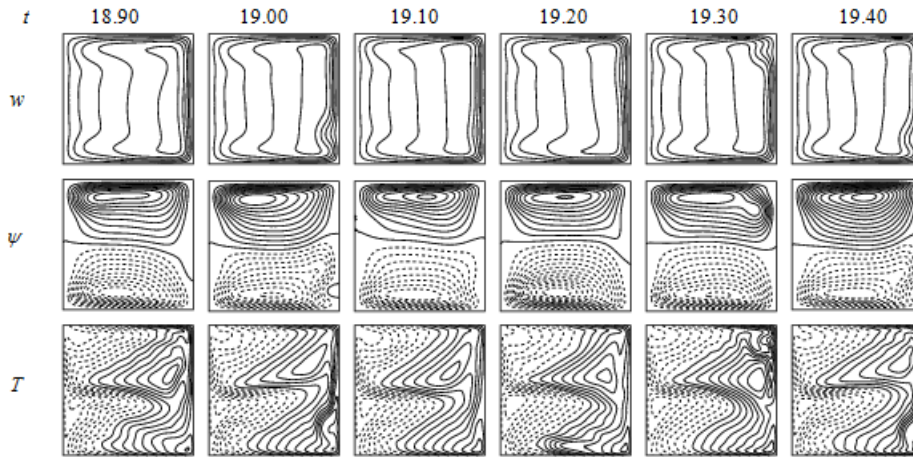


Fig. 10 Velocity contour (top & middle) and isotherm (bottom) for $Tr = 1450$

4.1.2. Case II: Counter- Rotation ($-1500 \leq Tr < 0$)

First, we realize the time-development of the US for $Tr = -30$, and it represents the multi-periodic oscillation as Fig. 11(a). PS is further plotted in Fig. 11(b) for explaining the multi-periodicity properly.

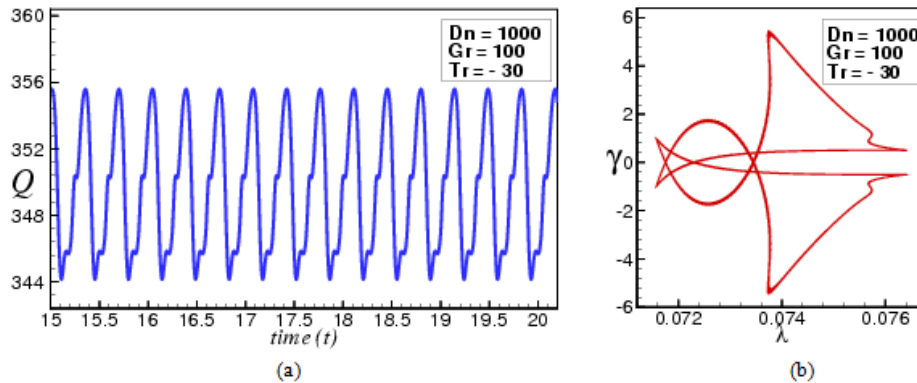


Fig. 11 Transient solution for $Tr = -30$ (a) Q as a function of time, (b) PS of (a)

It is demonstrated that the path lines of the PS coincide at the starting point after completing two cycles. Flow velocity (axial velocity), stream function and corresponding isotherms are exhibited in Fig. 12. AF patterns describe that, when two-vortex asymmetric solutions are formed, the flow velocity is towards the concave wall of the system ($t = 17.70$). It is obtained that the axial velocity forms a dumbbell shape at the right side of the contour ($t = 17.60$) and as a consequence, another vortex has appeared in the lower part of the duct. At time $t = 17.80$, SF consists of 4-vortex solution for generating the maximum-velocity regime. It is also observed that at $t = 17.90$, two maximum-velocity regimes are found where the area of upward part is smaller than the area of below part and the single dumbbell appeared at the

bottom wall; for this reason, the lower vortex is larger than the upper one, resulting in a four-vortex secondary flow. The isotherms illustrate that when the AF does not produce maximum-velocity regime, the density of the isotherm stream is less but the opposite criteria are found when AF generates the maximum-velocity regimes. So, it can be easily said that the AF definitely affects the secondary vortex including isotherms.

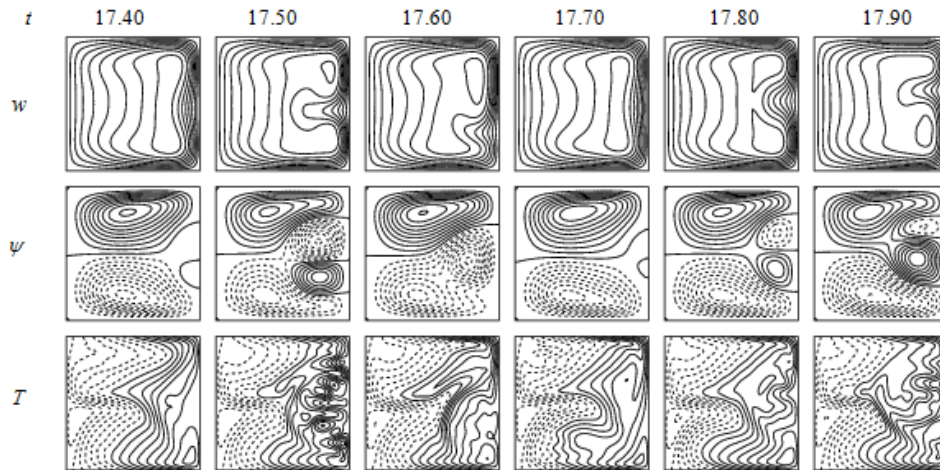


Fig. 12 Velocity contour (top & middle) and isotherm (bottom) for $Tr = -30$

With further increase of Tr in the negative direction, another flow transformation occurs at $Tr = -160$, where the multi-periodic flow shifts to a steady-state flow. It should be mentioned here that the steady-state flow initiates at $Tr = -160$ and terminates at $Tr = -390$ as found from the linear stability analysis. Fig. 13(a) displays the steady-state solution at $Tr = -230$. Flow characteristics including axial velocity, stream function and isotherms are visualized in Fig. 13(b), where 4-vortex symmetric secondary vortices are noted for the steady-state solution.

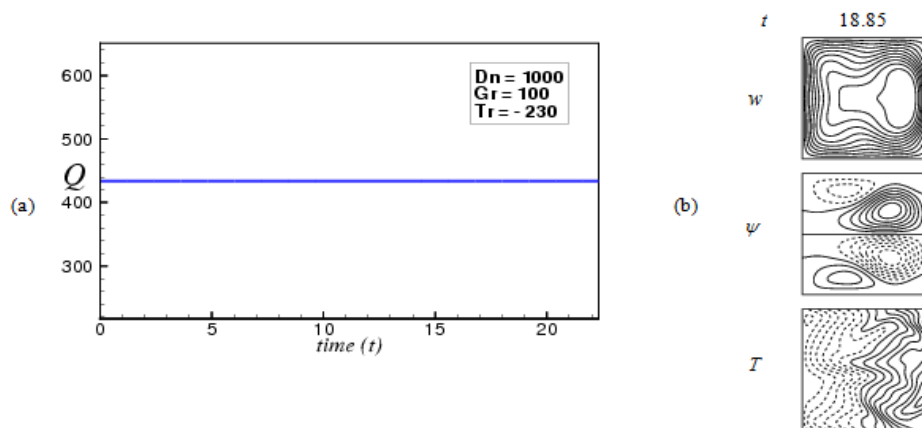


Fig. 13 Transient solution for $Tr = -230$ (a) Q as a function of time, (b) Velocity contour (top & middle) and isotherm (bottom) for $Tr = -230$

When the values of Tr are gradually increased at $Tr = -400$, the steady-state flow turns into a multi-periodic flow (Fig.14 (a)). The PS of the multi-periodic flow is represented in Fig. 14(b), which shows that the streamlines have two multiple orbits before they converge at the starting point. Axial velocity, stream function and isotherms are revealed in Fig. 15. Interesting types of flow properties are found at $Tr = -400$. The AF has pushed to the right side of the contour. The secondary vortices of the flow patterns depict that due to the Coriolis force in the negative direction the dotted lines are produced at the duct's ceiling wall and the solid lines are created at the duct's bottom wall. As a consequence of these types of rotation of negatively, the Ekman vortices have originated at the duct's interior portion. Here, there is also a relationship established between axial velocity, stream function, and isotherms. For example, at $t = 14.45$, a pair of high-velocity regions with double dumbbells of axial flow are produced at the duct's interior side; hence in a four-vortex secondary flow is generated where the two new vortices are generated at the duct's interior side. Besides, the dumbbells of the bottom side of axial flow are, for this reason, smaller than those at the upper one. Although the

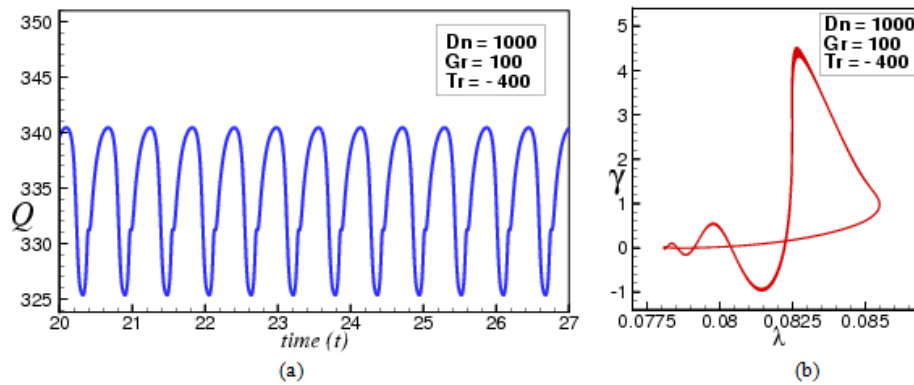


Fig. 14 Transient solution for $Tr = -400$ (a) Q as a function of time, (b) PS of (a)

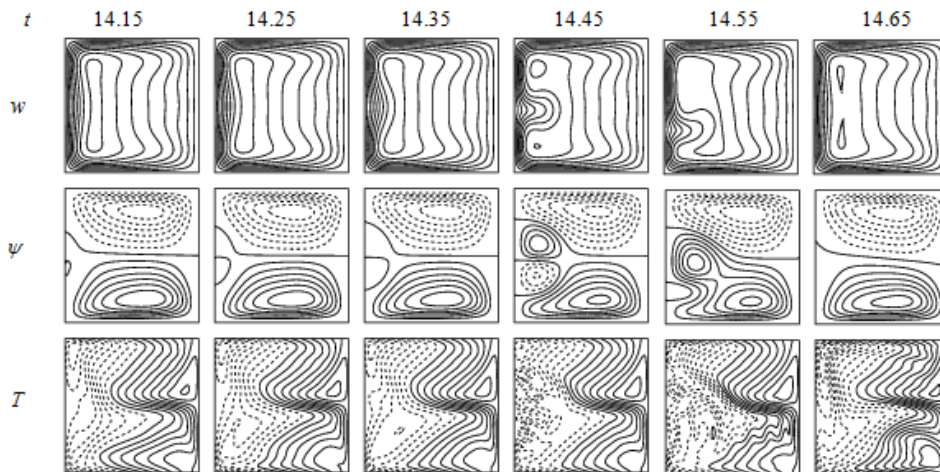


Fig. 15 Velocity contour (top & middle) and isotherm (bottom) for $Tr = -400$

two vortices look similar, the vortex of the part below is smaller than that of the upward part. However, in brief, despite of changing direction of the axial velocity, the meaning of flow characteristics is the same as in axial and secondary flow. Mainly, the flow velocity direction changes because of the duct rotation. It is noted that the fluid mixing and total heat distribution in the flow are undoubtedly affected by the change in direction of the flow rate.

Now, we manifest the transitional characteristics of the flow at $Try = -730$. Fig. 16(a) shows a steady-state solution. Axial flow, stream function and isotherms are explored in Fig. 16(b).

If the Coriolis force is more raised at $Try = -1100$, the steady-state solution jumps to the periodic oscillation (see Fig. 17(a)). Speaking more clearly about regular oscillation, PS is enumerated as drawn in Fig. 17(b) which deliberates that the stream lines meet at the starting point after completing an orbit. The AF and SF and isotherms are shown in Fig. 18. Then, we further explore unsteady characteristics for $Try = -1450$. It is narrated that the time evolution delivers irregular oscillation as shown in Fig. 19 (a). To have a better understanding of the flow movement, PS is also calculated as depicted in Fig. 19(b). According to PS, it is analyzed that the direction of the stream flow moves arbitrarily in the $\lambda - \gamma$ plane, and the line spectrums oscillate continuously. Fig. 20 displays AF, SF and isotherms where it is seen that 2- to 4-vortex solutions are found at $Try = -1450$ where the dotted lines are seen in the top wall and the additional vortices are situated in the inner wall of the duct. At $t = 19.10$ for $Try = -1450$, axial flow regions are created at the top, so that the secondary vortices are formed below. When 4-vortex solutions are found the axial flows are divided into two high-velocity regions and the fluids are mixed up more than those of the two-vortex solution as also shown by the temperature profiles. So, USs do not demonstrate only the time-dependent solutions but also disclose a connection between the liner stability, axial flows, secondary flows and the heat transfer.

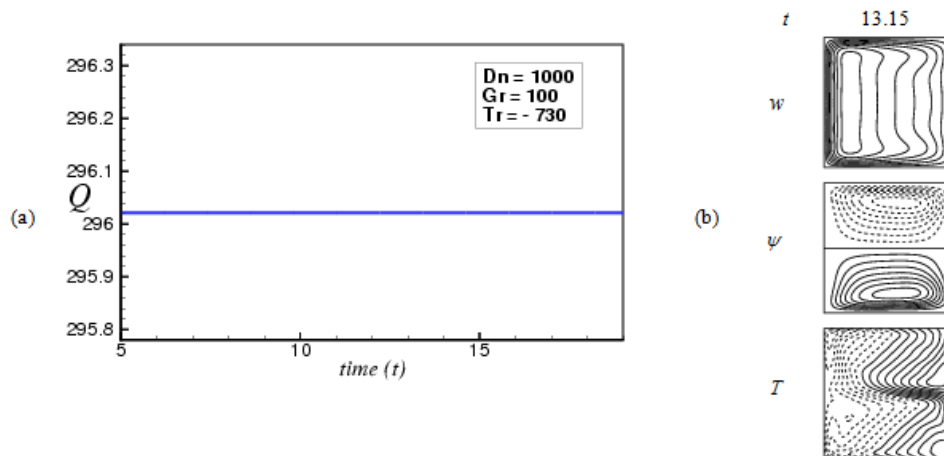


Fig. 16 Transient solution for $Try = -730$ (a) Q as a function of time, (b) Velocity contour (top & middle) and isotherm (bottom)

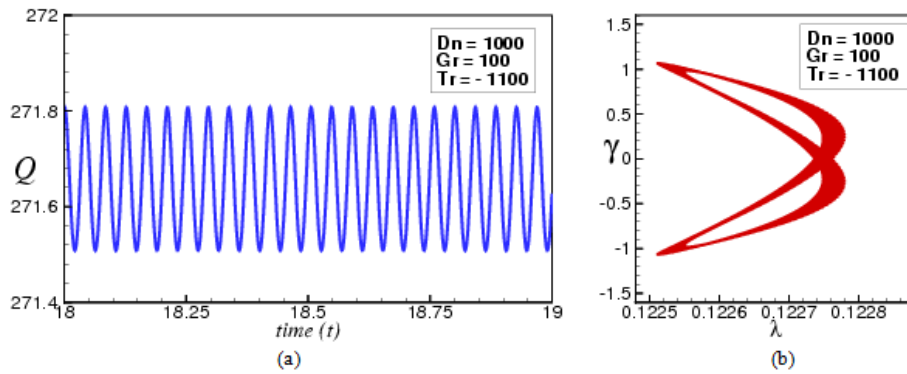


Fig. 17 Transient solution for $Tr = -1100$ (a) Q as a function of time (b) PS of (a)

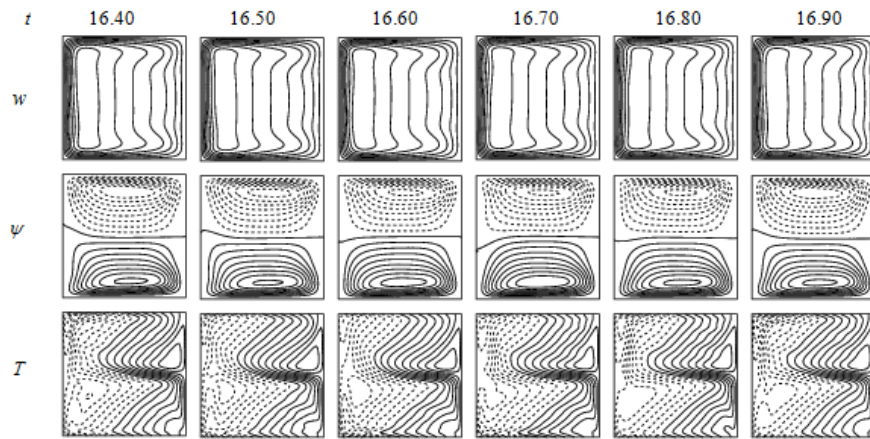


Fig. 18 Velocity contour (top and middle) and isotherm (bottom) for $Tr = -1100$

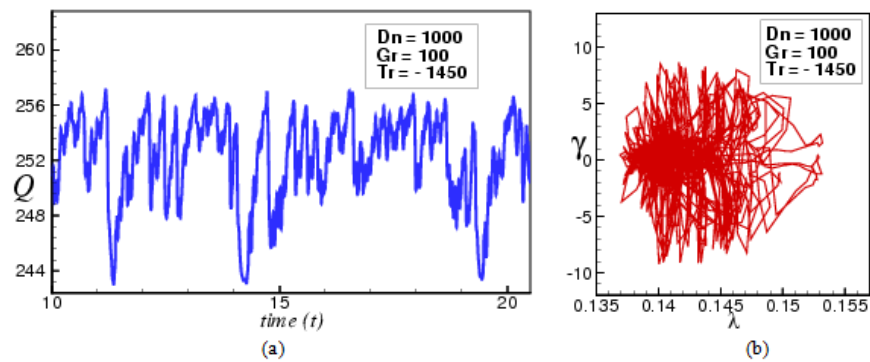


Fig. 19 Transient solution for $Tr = -1450$ (a) Q as a function of time (b) PS of (a)

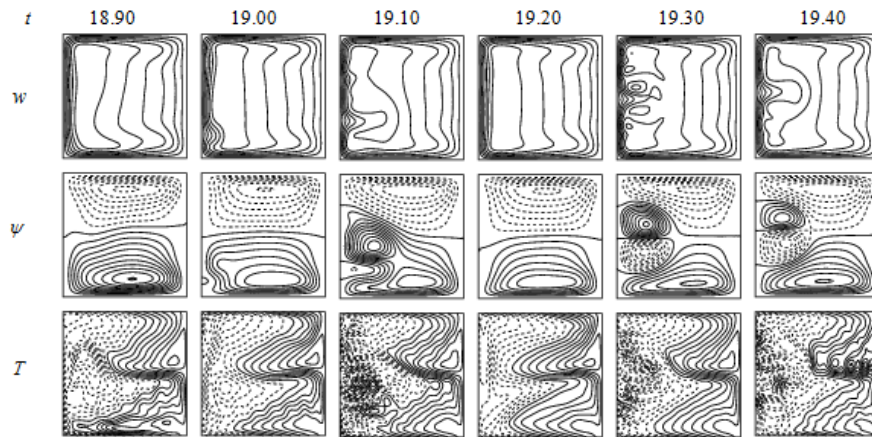


Fig. 20 Velocity contour (top & middle) and isotherm (bottom) for $Tr = -1450$

4.2. Vortex generation of unsteady solutions

Now, the observation of the number of vortices of US for monitoring varying Tr is performed by the bar diagram. Fig. 21 presents the variation of θ at $\delta = 0.015$ and Tr varying from -1500 to 1500 in the $(Tr - \theta)$ plane. Also, 2- to 4-vortex solutions have been visible for varying value of Tr . The maximum numbers of vortices are produced for weak rotation causing the resulting force of Centrifugal, Coriolis and Buoyancy forces.

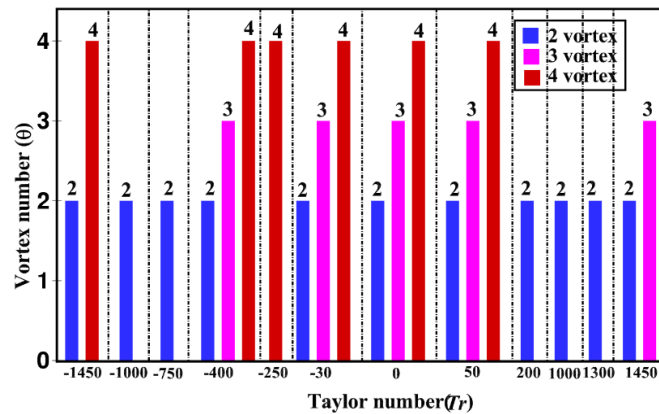


Fig. 21 Schematic diagram of USs at $\delta = 0.015$

4.3. Heat Transfer

Heat transfer (HT) through the duct for both rotation (co-rotation and counter-rotation) is calculated as shown in Figs. 22(a) and 22(b), respectively. Here, the cooling and heating sidewalls are achieved from the time-independent (steady branch) solution which is marked by the solid lines. The symbols are determined by taking the time average of the US for constant Tr .

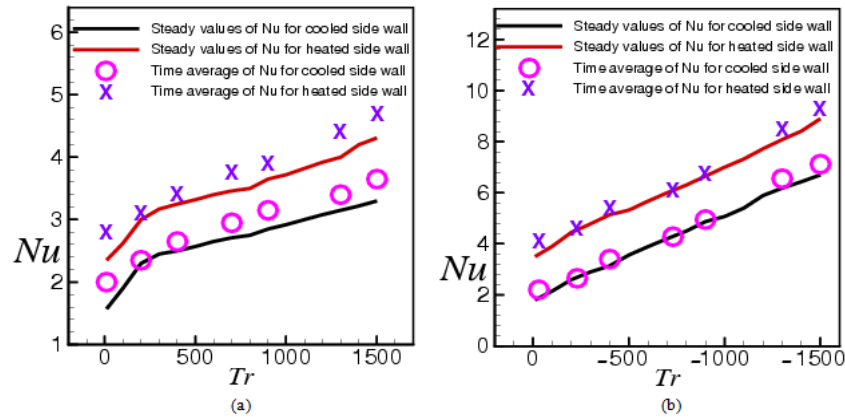


Fig. 22 Nusselt number variation for varying Tr : (a) positive rotation, (b) negative rotation

It is clearly shown, in the above two figures, that the average Nusselt number for cooled and heated side walls follows approximately linear trend with increasing Tr in the negative direction while a slightly curved trend is in the positive direction. So, the heat is transferred for negative rotation more than for positive one for both cooling and heating walls. The cause of it is the duct rotation. Moreover, because of the advection in the duct, time-average of the transient flow at the cooling sidewall passes less heat than that at the cooling wall. In addition, the flow transition and heat transfer throughout the duct are related to each other. The steady-state in the time-dependent flow transfers less heat than the regular and irregular oscillation. This has occurred because of fluid fixing. More precisely, in comparison to the steady-state solution, the flows vibrate more at periodic, multi-periodic, and chaotic oscillations. As a result, the fluid particles collide with each other and enhance heat transfer.

4.4 Validation of the Study

Here, a comparative study between the numerical and experimental investigations has been provided for both curved square duct (CSD) flow so as to validate our current study. There are numerous authors who have disclosed the experimental outcomes of the curved square duct flow. Yamamoto et al. [43] investigated experimentally the rotating curved square duct flow. They adopted the visualization technique to explore the experimental outcome with a constant curvature $\delta = 0.3$. Yamamoto et al. [43] used a water flow tank where the dye was injected continuously and this dye was adjusted by the alcohol to be the same as the weight of water. At first, they fixed the positive rotation at $Tr = 150$ and took photographs at an angle 180° inlet for several values of Dn . The same work was then conducted for negative rotation at $Tr = -150$. In the present study, we fix our parameters according to Yamamoto et al [43] experiments. Then we obtain the numerical outcome of the secondary flow for several values of Dn as shown in Fig. 23 which shows a perfect match between our numerical computations and investigational outcomes.

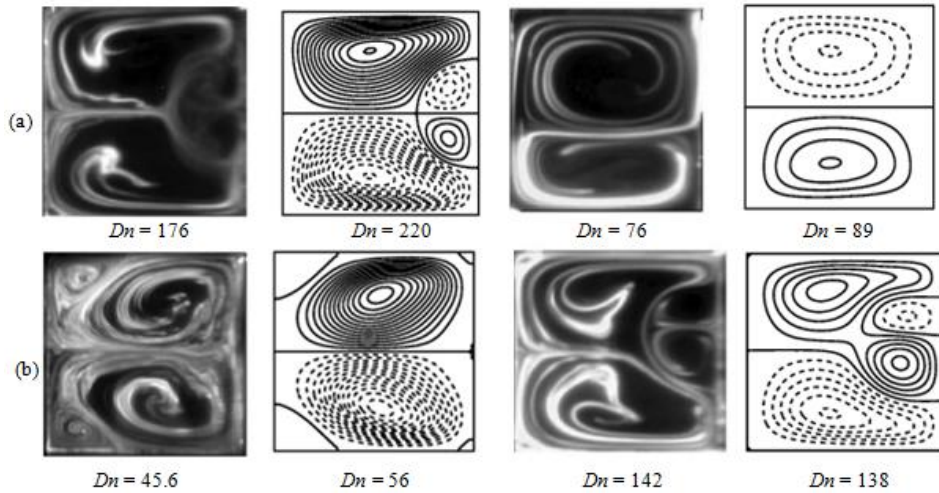


Fig. 23 Experimental (left, Yamamoto et al. [43]) vs. numerical (right, authors) results for rotating curved square duct flow; (a) $Tr = 150$, (b) $Tr = -150$

5. DISCUSSIONS

There is a large interest of engineering community in studying the flow characteristics in a curved system because it has a wide range of real-life applications including heat exchangers, chemical mixing, power industry, rotating electrical machinery etc. as well as other application areas such as blood flow in human veins and arteries. The researchers are, therefore, interested in investigating different types of phenomena by changing the governing equations. Here, we discuss contributions and limitations of some papers published in literature and try to explain what is new in the ongoing exploration. Yang et al. [44] used CFD based Fluent software and user-defined function to expose flow vibration and time-dependent flow configuration through a circular cylinder. Khanafer et al. [45] conducted Nk5000 code to explore the effect in streamlines and isotherms with changing parameters and showed that the rotational speed expressively enhances overall heat throughout the fluid than other parameters such as Ri and Re number. Geike [46] reported the cavitation phenomena in the viscoelastic fluid flows. Dolon et al. [47] studied the flow analyses as well as the centrifugal influence in the duct size. Mousavi et al. [48] conducted nanofluid and thermal radiation through a needle to narrate the velocity ratio for the change of magnetic parameters. Bibin et al. [49] used vector plot to represent the axial velocity and showed temperature contour at several axial locations. Umavathi and Beg [50] applied finite difference method to demonstrate viscous and buoyancy effects in the secondary and isotherm contour for temperature different fluid through a vertical duct. Nobari et al. [51] analyzed the behavior of AF and SF pattern in annular duct at different inlets. They also calculated heat transfer in the duct but they did not visualize the isotherm variation in their exploration. Riyi et al. [52] elucidated heat transport and temperature profiles in the inner and outer inlet of the curved annular duct experimentally for a large range of Re. Mansour et al. [53] discussed the fluid mixing in three different tubes for several Dn over a large

range of the Re but their research did not provide any discussion of flow velocity or fluid mixing contours. Tanweer et al. [54] performed transitional behaviors with respect to several coefficients and observed heat transfer when the cylinder is near the moving wall. Though their study discussed heat transfer in a three-dimensional coordinate system, the investigation is limited for low Reynolds number. Hasan et al. [55-57] adopted spectral technique to explore time-dependent flow characteristics across the circular and non-circular channels including centrifugal and body force effects. However, no study is published so far that describes hydrothermal behavior of transient flow characteristics and energy distribution with forced convection in a curved square geometry with the effects of rotation, namely, the study which is successfully accomplished in this paper. Besides, a relationship among the axial velocity, stream function and isotherms is presented, and it is revealed that HT is enhanced substantially with increasing rotation, which has not been mentioned in the literature till now. The present study may improve the heat generation and transmission knowledge that constitute a new epoch in related fields to produce energy-related machinery.

6. CONCLUSION

The continuing study determines a spectral-based numerical approach on fluid flow and heat transfer through a CSD at rotating stage with a small curvature considering the bottom wall heating and the top wall cooling, the sidewalls are well insulated to prevent any heat loss. A wide-range of the Taylor numbers (Tr) ranging from - 1500 to 1500 is considered for different curvature ratio 0.015 and aspect ratio 1. The numerical findings are validated with the available experimental data. The following conclusions are drawn from the present study:

- Time-development flow as well as phase-space of the time progression results shows that the transient flow endures in the consequence “*multi-periodic* → *steady state* → *periodic* → *multi-periodic* → *chaotic*”, if Tr is increased in the positive direction; for negative rotation, however, the flow experiences the evolution: “*multi-periodic* → *steady state* → *multi-periodic* → *steady state* → *periodic* → *chaotic*”.
- Flow instability at negative rotation shows more transiency than that at positive rotation, and it is found that the regular and irregular oscillation at high rotation becomes stronger than that at small rotation.
- 2- to 6-vortex solutions are generated at the periodic, multi-periodic and chaotic flows, and the number of secondary vortices is significantly higher for the chaotic solutions while few for the steady-state solution.
- A strong bond between the AF and SF has been established for regular and irregular oscillation which agrees well with temperature distribution. The study shows that heat transfer occurs prominently if the rotation is increased either in the positive or in the negative direction.
- A strong dominance among heating-induced buoyancy force and centrifugal-Coriolis instability is observed that augments flow interaction and enriches heat transfer in the flow. The study reveals that chaotic solutions boost heat transfer more effectively than the steady-state or other physically realizable solutions due to formation of significant number of Dean vortices at the outer concave wall.

Acknowledgements: *The authors are very much grateful to the unanimous reviewers as well as the journal itself, namely those who have spent their valuable time to review the article fast and helped us to improve the quality and comprehensiveness of the article with constructive comments.*

REFERENCES

1. Mondal, R.N., Kaga, Y., Hyakutake, T., Yanase, S., 2006, *Effects of curvature and convective heat transfer in curved square duct flows*, Trans ASME, Journal of Fluids Engineering, 128(9), pp. 1013-1022.
2. Mondal, R.N., Kaga, Y., Hyakutake, T., Yanase, S., 2007, *Bifurcation diagram for two-dimensional steady flow and unsteady solutions in a curved square duct*, Fluid Dynamics Research, 39, pp. 413-446.
3. Yanase, S., Mondal, R.N., Kaga, Y., 2005, *Numerical Study of Non-Isothermal Flow with Convective Heat Transfer in a Curved Rectangular Duct*, International Journal of Thermal Science, 44(11), pp. 1047-1060.
4. Rumsey, C.L., Gatski, T.B., Morrison, J.H., 2010, *Turbulence Model Predictions of Strongly Curved Flow in a U-Duct*, AIAA Journal, 38(8), pp. 1394-1402.
5. Chandratilleke, T.T., Nadim, N., Narayanaswamy, R., 2013, *Analysis of Secondary Flow Instability and Forced Convection in Fluid Flow through Rectangular and Elliptical Curved Ducts*, Heat Transfer Engineering, 34(14), pp. 1237-1248.
6. Ahmadloo, E., Sobhanifar, N., Hosseini, F.S., 2014, *Computational Fluid Dynamics Study on Water Flow in a Hollow Helical Pipe*, Open Journal of Fluid Dynamics, 4(2), pp. 133-139.
7. Liu, F., Wang, L., 2009, *Analysis on multiplicity and stability of convective heat transfer in tightly curved rectangular ducts*, International Journal of Heat and Mass Transfer, 52(25-26), pp. 5849-5866.
8. Yanase, S., Kaga, Y., Daikai, R., 2002, *Laminar flow through a curved rectangular duct over a wide range of aspect ratio*, Fluid Dynamics Research, 31(3), pp. 151-83.
9. Yanase, S., Watanabe, T., Hyakutake, T., 2008, *Traveling-wave solutions of the flow in a curved-square duct*, Physics of Fluids, 20(12), 124101.
10. Nazeer, G., Islam, S., Shigri, S.H., Saeed, S., 2019, *Numerical investigation of different flow regimes for multiple staggered rows*, AIP Advances, 9(3), 035247.
11. Zhou, B., Wang, X., Guo, W., Gho, W.M., Tan, S.K., 2015, *Control of flow past a dimpled circular cylinder*, Experimental Thermal and Fluid Science, 69, pp. 19-26.
12. Zhang, J., Chen, H., Zhou, B., Wang, X., 2019, *Flow around an array of four equispaced square cylinders*, Applied Ocean Research, 89, pp. 237-250.
13. Hashemi, A., Fischer, P.F., Loth, F., 2018, *Direct numerical simulation of transitional flow in a finite length curved pipe*, Journal of Turbulence, 19(8), pp. 664-682.
14. Zhang, W., Wei, Y., Dou, H.S., Zhu, Z., 2018, *Transient behaviors of mixed convection in a square enclosure with an inner impulsively rotating circular cylinder*, International Communications in Heat and Mass Transfer, 98, pp. 143-154.
15. Wang, L., Yang, T., 2005, *Periodic oscillation in curved duct flows*, Physica D, 200, pp. 296-302.
16. Arpino, F., Cortellessa, G., Mauro, A., 2015, *Transient Thermal Analysis of Natural Convection in Porous and Partially Porous Cavities*, Numerical Heat Transfer, Part A: Applications, 67(6), pp. 605-631.
17. Mondal, R.N., Islam, M.S., Uddin, K., Hossain, M.A., 2013, *Effects of aspect ratio on unsteady solutions through curved duct flow*, Applied Mathematics and Mechanics, 34(9), pp. 1107-1122.
18. Ray, S.C., Hasan, M.S., Mondal, R.N., 2020, *On the Onset of Hydrodynamic Instability with Convective Heat Transfer Through a Rotating Curved Rectangular Duct*, Mathematical Modelling of Engineering Problems, 7(1), pp. 31-44.
19. Hasan, M.S., Islam, M.M., Ray, S.C., Mondal, R.N., 2019, *Bifurcation structure and unsteady solutions through a curved square duct with bottom wall heating and cooling from the ceiling*, AIP Conference Proceedings, 2121, 050003.
20. Hasan, M.S., Mondal, R.N., Lorenzini, G., 2019, *Numerical Prediction of Non-isothermal Flow with Convective Heat Transfer through a Rotating Curved Square Channel with Bottom Wall Heating and Cooling from the Ceiling*, International Journal of Heat and Technology, 37(3), pp. 710-726.
21. Islam, M.Z., Mondal, R.N., Rashidi, M.M., 2017, *Dean-Taylor Flow with Convective Heat Transfer through a Coiled Duct*, Computers and Fluids, 149, pp. 141-155.
22. Kurtulmus, N., Zontul, H., Sahin, B., 2020, *Heat transfer and flow characteristics in a sinusoidally curved converging-diverging channel*, International Journal of Thermal Sciences, 148, 106163.
23. Zheng, Y., Jiang, P.X., Luo, F., Xu, R.N., 2019, *Instability during transition to turbulence of supercritical pressure CO₂ in a vertical heated serpentine tube*, International Journal of Thermal Sciences, 145, 105976.
24. Dean, W.R., 1927, *Note on the motion of fluid in a curved pipe*, Philos Mag., 4, pp. 208-23.

25. Ozaki, K., Maekawa, H., 2004, *Curvature Effects in the Curved Duct for the Compressible Viscous Flow*, 24th International Congress of the Aeronautical Sciences, pp. 1787-1792.
26. Chandratilleke, T.T., Nadim, N., Narayanaswamy, R., 2012, *Vortex structure-based analysis of laminar flow behaviour and thermal characteristics in curved ducts*, International Journal of Thermal Sciences, 59, pp. 75-86.
27. Alam, M.M., Ota, M., Ferdows, M., Islam, M.N., Wahiduzzaman, M., Yamamoto, K., 2007, *Flow through a rotating helical pipe with a wide range of the Dean number*, Arch. Mech., 59(6), pp. 501-517.
28. Bayat, P., Rezai, P., 2017, *Semi-Empirical Estimation of Dean Flow Velocity in Curved Microchannels*, Scientific Reports, 7, 13655.
29. Li, Y., Wang, X., Yuan, S., Tan, S.K., 2016, *Flow development in curved rectangular ducts with continuously varying curvature*, Experimental Thermal and Fluid Science, 75, pp. 1-15.
30. Watanabe, T., Yanase, S., 2013, *Bifurcation Study of Three-Dimensional Solutions of the Curved Square-Duct Flow*, Journal of the Physical Society of Japan, 82, 074402.
31. Nowruzi, H., Ghassemi, H., Nourazar, S.S., 2020, *Study of the effects of aspect ratio on hydrodynamic stability in curved rectangular ducts using energy gradient method*, Engineering Science and Technology, 23(2), pp. 334-344.
32. Norouzi, M., Biglari, N., 2013, *An analytical solution for Dean flow in curved ducts with rectangular cross section*, Physics of Fluids, 25, 053602.
33. Razavi, S.E., Soltanipour, H., Choupania, P., 2015, *Second Law Analysis of Laminar Forced Convection in a Rotating Curved Duct*, Thermal Science, 19(1), pp. 95-107.
34. Hasan, M.S., Mondal, R.N., Lorenzini, G., 2019, *Centrifugal Instability with Convective Heat Transfer Through a Tightly Coiled Square Duct*, Mathematical Modelling of Engineering Problems, 6(3), pp. 397-408.
35. Hasan, M.S., Mondal, R.N., Kouchi, T., Yanase, S., 2019, *Hydrodynamic instability with convective heat transfer through a curved channel with strong rotational speed*, AIP Conference Proceedings, 2121, 030006.
36. Sasmito, A.P., Kurnia, J.C., Mujumdar, A.S., 2011, *Numerical evaluation of laminar heat transfer enhancement in nanofluid flow in coiled square tubes*, Nanoscale Research Letters, 6, 376.
37. AL-Juhaishi, L.F.M., Ali, M.F.M., Mohammad, H.H., Ajeel, R.K., 2020, *Numerical thermal-hydraulic performance investigations in turbulent curved channel flow with horseshoe baffles*, Heat transfer, 49(6), pp. 3816-3836.
38. Zhang, L.Y., Lu, Z., Wei, L.C., Yang, X., Yu, X.L., Meng, X.Z., Jin, L.W., 2019, *Numerical investigation of flow characteristics and heat transfer performance in curve channel with periodical wave structure*, International Journal of Heat and Mass Transfer, 140, pp. 426-439.
39. Zhang, C., Niu, Y., Xu, J., 2020, *An anisotropic turbulence model for predicting heat transfer in a rotating channel*, International Journal of Thermal Sciences, 148, 106119.
40. Schindler, A., Younis, B.A., Weigand, B., 2019, *Large-Eddy Simulations of turbulent flow through a heated square duct*, International Journal of Thermal Sciences, 135, pp. 302-318.
41. Gottlieb, D., Orazag, S.A., 1977, *Numerical Analysis of Spectral Methods*, Society of Industrial and Applied Mathematics, Philadelphia, USA.
42. Mondal, R.N., 2006, *Isothermal and Non-isothermal Flows through Curved ducts with Square and Rectangular Cross Sections*, Ph.D. Thesis, Department of Mechanical and Systems Engineering, Okayama University, Japan.
43. Yamamoto, K., Xiaoyum, W., Kazou, N., Yasutuka, H., 2006, *Visualization of Taylor-Dean flow in a curved duct of square cross section*, Fluid Dynamics Research, 38, pp. 1-18.
44. Yang, Z., Ding, L., Zhang, L., Yang, L., He, H., 2020, *Two degrees of freedom flow-induced vibration and heat transfer of an isothermal cylinder*, International Journal of Heat and Mass Transfer, 154, 119766.
45. Khanafer, K., Aithal, S.M., Vafai, K., 2019, *Mixed convection heat transfer in a differentially heated cavity with two rotating cylinders*, International Journal of Thermal Sciences, 135, pp. 117-132.
46. Geike, T., 2021, *Bubble dynamics-based modeling of the cavitation dynamics in lubricated contacts*, Facta Universitatis-Series Mechanical Engineering, 19(1), pp. 115-124.
47. Dolon, S.N., Hasan, M.S., Lorenzini, G., Mondal, R.N., 2021, *A computational modeling on transient heat and fluid flow through a curved duct of large aspect ratio with centrifugal instability*, The European Physical Journal Plus, 136, 382.
48. Mousavi, S.M., Rostami, M.N., Yousefi, M., Dinarvand, S., 2021, *Dual solutions for MHD flow of a water-based TiO₂-Cu hybrid nanofluid over a continuously moving thin needle in presence of thermal radiation*, Reports in Mechanical Engineering, 2(1), pp. 31-40.
49. Bibin, K.S., Jayakumar, J.S., 2020, *Thermal hydraulic characteristics of square ducts having porous material inserts near the duct wall or along the duct centre*, International Journal of Heat and Mass Transfer, 148, 119079.

50. Umavathi, J.C., Bég, O.A., 2020, *Effects of thermo-physical properties on heat transfer at the interface of two immiscible fluids in a vertical duct: Numerical study*, International Journal of Heat and Mass Transfer, 154, 119613.
51. Nobari, M.R.H., Ahrabi, B.R., Akbari, G., 2009, *A numerical analysis of developing flow and heat transfer in a curved annular pipe*, International Journal of Thermal Sciences, 48, pp. 1542–1551.
52. Riyi, L., Xiaoqian, W., Weidong, X., Xinfeng, J., Zhiying, J., 2019, *Experimental and numerical study on forced convection heat transport in eccentric annular channels*, International Journal of Thermal Sciences, 136, pp. 60-69.
53. Mansour, M., Thévenin, D., Zähringer, K., 2020, *Numerical study of flow mixing and heat transfer in helical pipes, coiled flow inverters and a novel coiled configuration*, Chemical Engineering Science, 221, 115690.
54. Tanweer, S., Dewan, A., Sanghi, S., 2020, *Influence of three-dimensional wake transition on heat transfer from a square cylinder near a moving wall*, International Journal of Heat and Mass Transfer, 148, 118986.
55. Hasan, M.S., Mondal, R.N., Lorenzini, G., 2020, *Physics of bifurcation of the flow and heat transfer through a curved duct with natural and forced convection*, Chinese Journal of Physics, 67, pp. 428-457.
56. Hasan, M.S., Islam, M.S., Badsha, M.F., Mondal, R.N., Lorenzini, G., 2020, *Numerical Investigation on the Transition of Fluid Flow Characteristics Through a Rotating Curved Duct*, International Journal of Applied Mechanics and Engineering, 25(3), pp. 45-63.
57. Hasan, M.S., Mondal, R.N., Lorenzini, G., 2020, *Coriolis force effect in steady and unsteady flow characteristics with convective heat transfer through a curved square duct*, International Journal of Mechanical Engineering, 5(1), pp. 1-39.